Work Function Engineering of Graphene Electrode *via* Chemical Doping

Yumeng Shi,[†,‡] Ki Kang Kim,[‡] Alfonso Reina,[§] Mario Hofmann,[‡] Lain-Jong Li,[⊥,*] and Jing Kong[‡,*]

[†]School of Materials Science and Engineering, Nanyang Technological University 50, Nanyang Avenue, Singapore 639798, [‡]Department of Electrical Engineering and Computer Sciences, Massachusetts Institute of Technology, Cambridge, Massachusetts 02139, [§]Department of Materials Science and Engineering, Massachusetts Institute of Technology, Cambridge, Massachusetts 02139, and [⊥]Research Center for Applied Science, Academia Sinica, Taipei, Taiwan 11529

ABSTRACT In this work, we demonstrate that graphene films synthesized by chemical vapor deposition (CVD) method can be used as thin transparent electrodes with tunable work function. By immersing the CVD-grown graphene films into $AuCl_3$ solution, Au particles were formed on the surface of graphene films by spontaneous reduction of metal ions. The surface potential of graphene films can be adjusted (by up to ~0.5 eV) by controlling the immersion time. Photovoltaic devices based on n-type silicon interfacing with graphene films were fabricated to demonstrate the benefit of an electrode with tunable work function. The maximum power conversion efficiency (PCE) achieved was ~0.08%, which is more than 40 times larger than the devices without chemical doping.

KEYWORDS: surface analysis · graphene · doping · photovoltaic devices

Indium tin oxide (ITO) has been widely used as electrodes in optoelectronic devices such as organic light-emitting diodes (OLEDs) and photovoltaic cells, due to its high transparency and good conductivity. The price of ITO has gone up significantly in recent years due to the limited indium resources. In addition, their chemical and electronic stability and mechanical flexibility limit their applications in flexible electronics.[1] With the emergence of novel flexible electronic devices, there is a growing demand for flexible electrodes, where conventional materials such as metal conductors and ITO may not reach the required bendability.

Two-dimensional networks of carbon nanotubes (CNTs) have been considered as a candidate to replace ITO because they possess excellent mechanical[2,3] and electrical properties.[4] Recently, there has been tremendous research in the two-dimensional crystal graphene and its derived nanomaterials.[5−8] Graphene sheets can be considered as an unzipped CNT, which has unique physical properties such as high carrier mobility,[5] long phase coherence length,[9] fractional quantum Hall effect,[10] bipolar supercurrent,[11] suppression of the weak localization,[12] deviation from the adiabatic Born−Oppenheimer approximation,[13] *etc*. On the basis of these unique electronic properties and the two-dimensional planar structure, graphene also appears as a promising material for transparent electrodes.[5,14,15] Furthermore, besides good conductivity and transparency of the electrode, the performance and current density for semiconducting electronic devices, such as light-emitting diodes and field-effect transistors, strongly rely on the carrier injection efficiency through the contact between electrodes and semiconducting material layers.[16,17] Therefore, the band alignment between electrodes and semiconductors and the surface property of the electrode have been an extensively investigated area.[18−20] Finding a certain conductive material with the desired work function for efficient carrier injection may sometimes be difficult. Both theoretical and experimental results have demonstrated that the Fermi energy shift of single-layer graphene (SLG) can be achieved through deliberate doping by aromatic molecules,[21,22] gas molecules,[23] or electrostatic gating.[5,24] These results suggest that controlling the work function of graphene electrodes is possible.

Tremendous progress has been achieved for the synthesis and characterization of graphene in the past few years.[25] Transparent graphene electrodes have been formed by either reducing graphene oxide[26] or a chemical bottom-up approach, where molecules of giant polycyclic aromatic hydrocarbons cross-link to form graphene nanosheets.[27] However, the conductivity of these films is still limited[28] and

*Address correspondence to jingkong@mit.edu, lanceli@gate.sinica.edu.tw.

Received for review March 17, 2010 and accepted April 21, 2010.

Published online April 30, 2010.
10.1021/nn1005478

high enough electrical conductivity is required for good electrodes.

Recently, it has been demonstrated that continuous large-area graphene thin films can be synthesized by vacuum graphitization and ambient pressure chemical vapor deposition (APCVD) methods.[29−34] In this contribution, we use graphene films formed by chemical vapor deposition (CVD-G) as an ultrathin transparent electrode. We demonstrated that the work function of graphene can be tuned by $AuCl_3$ doping. $AuCl_3$ is a commonly used compound in doping organic conductors. The Au^{III} can be reduced to Au particles by the charge transfer from graphene which results in p-type doping behavior of graphene. $AuCl_3$ has been chosen for the stability of its doping effect. The surface potential change of graphene as a function of doping time was studied by measuring the contact potential difference (CPD) using Kelvin probe microscopy. Silicon photovoltaic devices with graphene electrodes were fabricated as a demonstration of the advantages of using CVD-G electrodes with tunable work function.

RESULTS AND DISCUSSION

The images from the atomic force micrscopy (AFM) in Figure 1A−D and from scanning Kelvin probe microscopy (SKPM) in Figure 1A′−D′ show the effect of $AuCl_3$ doping time on the surface morphology and surface potential of CVD-G, respectively. With longer doping time, it was observed that the size of Au particles became larger and the morphology changed. The formation of Au particles on CVD-G can be understood from an electrochemical perspective since the reduction potential of $AuCl_4^-$ ion (1.0 V) is higher than the reduction potential of graphene (0.22 V).[35] In aqueous solutions, $AuCl_3$ forms a square planar complex, $AuCl_4^-$, and the following reaction takes place on graphene:[36]

$$AuCl_4^- + 3e \rightarrow Au^0 \downarrow + 4Cl^- \quad (1)$$

We noticed that for samples with 20 s doping time, the Au particles uniformly cover the surface of the graphene film. For less than 20 s doping, Au particles tend to form on the wrinkles and thicker layers of CVD-G.[37] As the doping time increases over 20 s, larger Au particles form and the size distribution of Au particles becomes broader. The SKPM images in Figure 1 indicate that the measured surface potential (V_{sur}) of Au particles is higher than adjacent graphene region (where color contrast is lower), and the V_{sur} difference between Au particles and graphene is from ~0.3 to ~0.8 V, depending on the Au particle size. The V_{sur} of Au particles is always more positive than that of adjacent graphene regions, suggesting that the doping caused by Au particles is p-type on graphene (*i.e.*, Au particles receive electrons from graphene), which is consistent with the chemical reaction 1. This hole doping process results in the work function shift of the CVD-G. Figure 1E plots

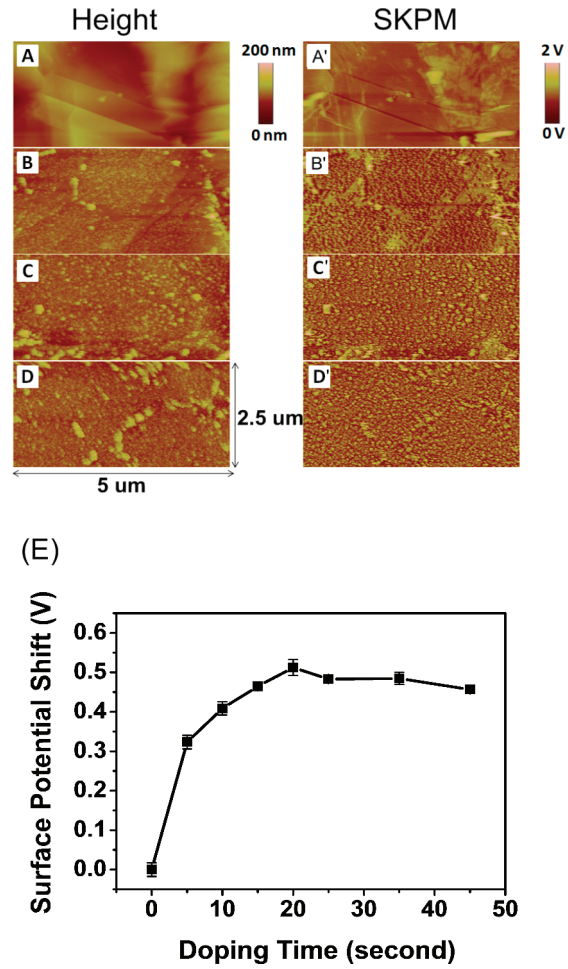

Figure 1. AFM images for as-grown CVD-G on 300 nm Ni (A) and those doped with $AuCl_3$ for (B) 5 s, (C) 25 s, (D) 45 s. (A′−D′) Corresponding SKPM images. (E) Surface potential CVD-G on Ni substrate as a function of $AuCl_3$ doping time.

the V_{sur} shift (ΔV_{sur}) *versus* various $AuCl_3$ doping times. Since the CPD method relies on the stability of the work function of AFM tips and is also sensitive to the measurement environment, such as humidity and electric grounding, we took the V_{sur} as the averaged value over an area of 1 μm × 1 μm and the as-grown CVD-G film was used as a standard reference. Thus, ΔV_{sur} value are relative to the pristine as-grown sample:

$$\Delta V_{sur} = V_{sur}(\text{sample after doping}) - V'_{sur}(\text{as-grown graphene}) \quad (2)$$

For doping time less than 20 s, V_{sur} monotonically increases with doping time to about 0.5 V, and as the doping time further increases, the V_{sur} reduces slightly. Thus SKPM data indicate that the work function of CVD-G can be tuned by chemical doping and exposing to $AuCl_3$ results in electrons being withdrawn from CVD-G by the formation of Au particles, which give rise to an up-shift of V_{sur}. The surface potential measurements were consistent with electric transport measurements of CVD-G field-effect transistors in our previous experiments.[38] The slight down-shift for longer doping

time is unclear at this stage and will be subject to further investigation. One mechanism could be the hygroscopic nature of $AuCl_3$ at higher concentrations. The water molecule could affect the charge transfer behavior between graphene and $AuCl_3$.

The benefit for having a transparent electrode with tunable work function will be demonstrated subsequently by enhancing the performance of a photovoltaic device. After CVD synthesis, the graphene films were transferred to n-Si substrates by coating a thin layer of PMMA on top of graphene film. The underlying Ni film was etched by Ni enchant (TFB commercial etchant from Transene). Then the graphene/PMMA film was transferred to $AuCl_3$ solution for chemical doping. After $AuCl_3$ doping, the sheet resistance of graphene film decreases from 400 to ~100 Ω/sq (see ref 37 for details). The device fabrication procedure is schematically shown in Figure 2. Using CVD synthesis and the PMMA transfer method, the size of graphene conducting film can be easily scaled up without a fundamental limit.

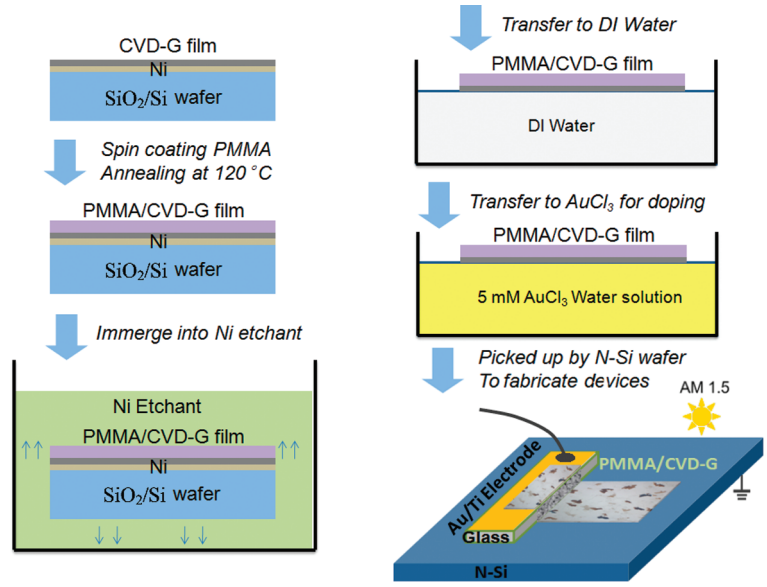

Figure 2. Schematic diagram of the transferring and device fabrication process. The graphene films are synthesized by an APCVD method on a SiO_2/Si wafer (300 nm thermal oxide) with 300 nm Ni film deposited in advance. The PMMA/CVD-G film was finally transferred to an n-type Si substrate for device fabrication.

Using the PMMA transferred CVD-G film, we fabricated photovoltaic diodes with a structure as shown in Figure 2. In order to demonstrate the effect of the work function shift on the device performance, the current density of several diodes under varying biases is compared in Figure 3A. These devices were measured with and without AM 1.5 illuminations for pristine CVD-G electrode and the CVD-G film with 20 s $AuCl_3$ doping. The devices show clear photovoltaic behaviors, which are similar to the previous reported work of carbon nanotube film/n-Si p−n junction solar cells.[39,40] Without illumination, both devices show a typical diode behavior, but the open circuit voltage (V_{oc}) and short circuit current (I_{sc}) are dramatically improved for the device with 20 s $AuCl_3$ doped CVD-G. More detailed AM 1.5 measurements for the devices with various doping time are shown in Figure 3B. The device containing the 20 s $AuCl_3$ doped CVD-G film displays the highest V_{oc} and I_{sc}. For longer doping times, both of the V_{oc} and I_{sc} drop and it can be noticed that for the sample with extremely long doping times, for example, 20 min, the electrical behavior shows no large difference to 30 s doping, which is consistent with the SKPM results. The device performance as a function of $AuCl_3$ doping time is plotted in Figure 3C. The device with 20 s $AuCl_3$ doping shows the best photovoltaic performance. This observation can be explained by the SKPM reults in Figure 1E. Figure 3D schematically demonstrated the effect of work function change of graphene electrodes on the device performance. The work function of graphene is as large as graphite, ~4.66 eV,[24,41−43] and our SKPM measurement shows that with $AuCl_3$ modification the work function of graphene film can be up-shifted within the range of 0.5 eV. It has been reported that a heterojunction can be formed between carbonaceous (or graphitic) thin films and n-type silicon.[44,45] Under photoillumination, electron and hole pairs are generated in n-Si, similar to the case of carbon nanotube/n-Si solar cell;[46] the photogenerated electrons are directed toward the n-Si, while holes are injected into the graphene electrodes, due to the built-in electric field at the Si/graphene junction. However, unlike p-type semiconducting carbon nanotube, here graphene is a zero band gap material and it is simply treated as a metal. Therefore, the open circuit voltage corresponds to the amount of forward bias on the solar cell due to the bias of the solar cell junction with the light-generated current. Similar to the case for metal-on Si Schottky barrier solar cell,[47] V_{oc} can be expressed as[48,49]

$$V_{oc} = n[q\Phi_B + (kT/q)\ln(I_s/A_eA^*T^2)] \quad (3)$$

where n is the diode ideality factor, Φ_B is the barrier hight, T is the working temperature, I_s is the diode saturation current, A_e and A^* are the contact area of the diode and the Richardson constant, respectively. Thus, the surface potential modification (or work function engineering) of graphene electrodes results in different barrier heights between Si and graphene, which provides tunability for the V_{oc} in the proposed n-Si/graphene photovoltaic devices. Besides the work function engineering effect, doping with Au particles affects the output characteristics of the photovoltaic device in several other ways. First, the doping also affects the carrier concentration of the graphene film, which further changes the sheet resistance of the graphene film.[37] A reduction in sheet resistance could also contribute to the change of short circuit current. Figure 3C clearly

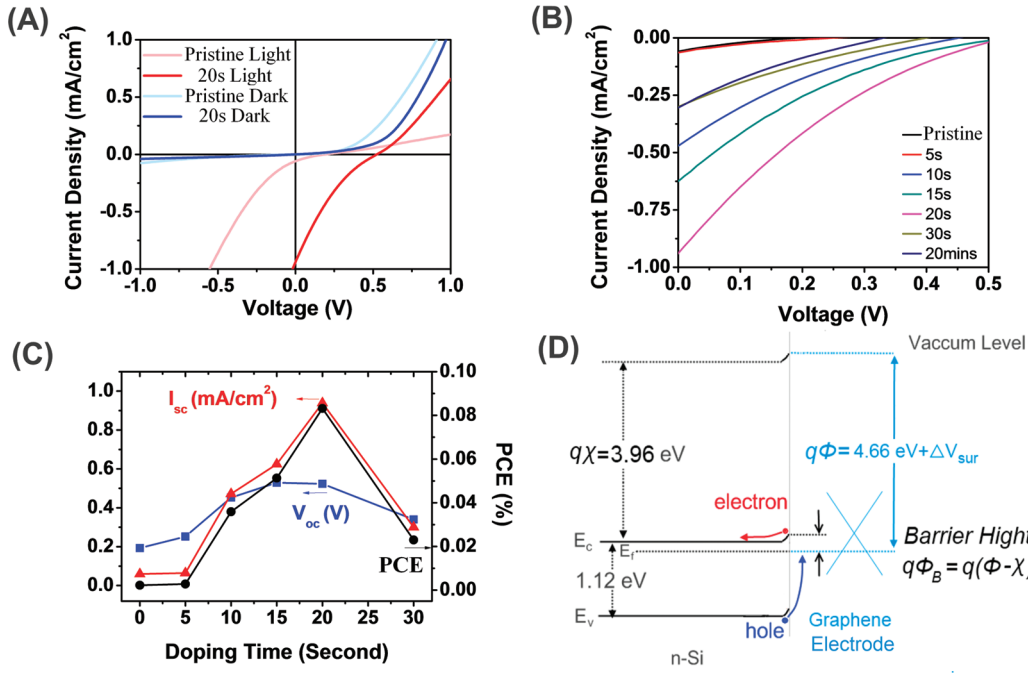

Figure 3. (A) Typical electrical measurement of pristine and 20 s $AuCl_3$ doped CVD-G/n-Si photovoltaic devices. (B) Current−voltage plots of the devices with different doping time from 5 s to 20 min under AM1.5 illumination. (C) Comparison of I_{sc}, V_{oc}, and PCE for different doping time. (D) Schematic illustration of the photovoltaic devices' band energy diagram (values obtained from ref 40).

shows the evolution of V_{oc}, I_{sc}, and power conversion efficiency (PCE) consistent with the V_{sur} shift in Figure 1E. Also, with a short $AuCl_3$ doping time, the Au particle layer is very thin, and the interface dipole between graphene and Au particles is expected to contribute strongly to the charge-injection process. With the increase of doping time, other effects such as transparency of the graphene film and the morphology-induced sheet resistance change need to be taken into consideration for device integration. A highest PCE achieved is ~0.08%, which is 40 times larger than the device without chemical doping. This value is comparable with the reported multiwalled CNT/n-Si solar cell devices.[40] It is suggested that the PCE of devices could be further improved by inserting a suitable p-type material between n-type Si and CVD-G electrodes or by opening the band gap of graphene. In summary, the chemical doping with Au particles can control the surface properties of graphene films, and the surface potential shift is able to explain the electrical characteristics for the diodes.

CONCLUSION

In conclusion, our EFM results show that the chemical doping of CVD-G with $AuCl_3$ causes a surface potential up-shift up to 0.5 eV, which is attributed to the hole doping process from Au particles. When n-type Si is covered by the CVD-G films, photoinduced charge seperation can be observed. The CVD-G electrodes offer more flexibilty in improving electric properties of the photovoltaic devices due to work function engineering. Our results suggest a new strategy for charge harvesting by graphene films. The detailed photoelectrical behaviors of CVD-G/semiconducting composite devices, particularly the graphene electrode contacts are worthy of further investigation. The capability of tailoring electrical properties of graphene is potentially useful for optoelectronics.

EXPERIMENTAL SECTION

Few-layer graphene (FLG) film was synthesized by CVD method using 300 nm Ni-coated Si/SiO_2 substrates. The Ni substrates were annealed in the CVD chamber with H_2 and Ar (H_2/Ar = 400:600 sccm) for 20 min at 1000 °C. CH_4 (4 sccm) along with H_2 (1400 sccm) was then flowed at 1000 °C for 5 min to carburize the Ni film. Finally, the Ni film was cooled to 500 °C with a cooling rate of 5 °C/min under $CH_4/H_2/Ar$ = 4:700:700 sccm, in order to control the thickness of graphene films. For the as-grown FLG films, one or two graphene layers were formed in most areas (see Supporting Information Figure S1). Details on the graphene film growth were reported elsewhere.[32,33] Atomic force microscopy (AFM), Raman spectroscopy, and transmission electron microscopy (TEM) techniques were used to characterize the CVD-synthsized FLG as described in refs 32 and 33. After CVD-G growth, the sample was immersed into $AuCl_3$ aqueous solution with a concentration of 5 mM for various durations. Then the sample was rinsed with DI water and blow-dried by nitrogen gas. In order to have a better grounding, the bottom Ni layer was not removed for the sample used for SKPM measurement.

The surface potential (V_{sur}) of CVD-G before and after doping with $AuCl_3$ was measured by a dual-pass technique in tapping mode using the scanning Kelvin probe method (SKPM) based on an AFM system Dimension 3000 from Veeco Metrology Group with NanoScope Signal Access Module. The measurement was conducted in air with Olympus (OMCL-AC240TM) Pt-

coated cantilevers. The tip curvature radius is ~15 nm, quality factor ~190, spring constant 2 N/m, resonance frequency ~70 kHz, and cantilever length 240 μm. The CPD value between tip and sample surface was taken as the averaged value over an area of 1 μm × 1 μm. The standard deviation of the experiment was 10 mV.

The surface potential study was performed by a dual-pass technique in tapping mode. Topography information (AFM image) was acquired in the first scan; the second scan was then performed while the tip was maintained at a constant distance (10 nm above the sample surface). Both a DC signal and an AC signal at the resonant frequency of the cantilever are applied to the metal-coated AFM probe while the tip is lifted up. If a potential difference (ΔV_{sur}) exists between the tip and the sample surface, the signal creates a varying electrostatic force, causing an oscillating motion in the cantilever. The ΔV_{sur} is measured by adjusting the DC voltage until there is no DC potential difference. The DC voltage is recorded as the CPD value.

Photovoltaic devices were fabricated based on n-Si substrate with a resistivity around 5 Ω · cm. The as-grown CVD-G film was coated with a thin layer of PMMA (~100 nm) by spin coating to avoid the breaking of graphene film.[50] After etching the underlying polycrystalline Ni with Ni etchant, the PMMA/CVD-G film was transferred to DI water or additionally 5 mM $AuCl_3$ aqueous solution for chemical doping. After that, the film was transferred back to water and suspended on the surface of DI water. The film was later picked up by an n-type silicon substrate with an attached insulating glass cover slide. Ti (10 nm) and Au (200 nm) were evaporated on the top side of the glass slide in advance, which forms the upper electrode connects to the PMMA/CVD-G film. The rest of the PMMA/CVD-G film was brought in firm contact with the Si surface after careful blow drying with N_2 gas. The bottom electrodes were formed by connecting electrical wires to the back side of Si using silver paint. The area of the PMMA/CVD-G film on top of Si is 3 mm × 3 mm. The photovoltaic devices were irradiated under a solar simulator at AM 1.5 with a light intensity of 100 mW. Electrical testing was performed by an Agilent 4156C precision semiconductor parameter analyzer.

Acknowledgment. Y.S. and L.-J.L. acknowledge the support by Nanyang Technological University and the support in part from National Research Foundation (Singapore, NRF-CRP-07-2). J.K. acknowledges the support by the Center for Excitonics, an Energy Frontier Research Center funded by the U.S. Department of Energy, Office of Science, Office of Basic Energy Sciences under Award Number DE-SC0001088.

Supporting Information Available: Figure S1. This material is available free of charge *via* the Internet at http://pubs.acs.org.

REFERENCES AND NOTES

1. Chen, Z.; Cotterell, B.; Wang, W.; Guenther, E.; Chua, S. J. A mechanical assessment of flexible optoelectronic devices. *Thin Solid Films* **2001**, *394*, 202–206.
2. Lu, J. P. Elastic properties of carbon nanotubes and nanoropes. *Phys. Rev. Lett.* **1997**, *79*, 1297–1300.
3. Popov, V. N.; Van Doren, V. E.; Balkanski, M. Elastic properties of single-walled carbon nanotubes. *Phys. Rev. B* **2000**, *61*, 3078–3084.
4. Ebbesen, T. W.; Lezec, H. J.; Hiura, H.; Bennett, J. W.; Ghaemi, H. F.; Thio, T. Electrical conductivity of individual carbon nanotubes. *Nature* **1996**, *382*, 54–56.
5. Novoselov, K. S.; Geim, A. K.; Morozov, S. V.; Jiang, D.; Zhang, Y.; Dubonos, S. V.; Grigorieva, I. V.; Firsov, A. A. Electric field effect in atomically thin carbon films. *Science* **2004**, *306*, 666–669.
6. Geim, A. K.; Novoselov, K. S. The rise of graphene. *Nat. Mater.* **2007**, *6*, 183–191.
7. Geim, A. K. Graphene: status and prospects. *Science* **2009**, *324*, 1530–1534.
8. Rao, C. N. R.; Sood, A. K.; Voggu, R.; Subrahmanyam, K. S. Some novel attributes of graphene. *J. Phys. Chem. Lett.* **2010**, *1*, 572–580.
9. Miao, F.; Wijeratne, S.; Zhang, Y.; Coskun, U. C.; Bao, W.; Lau, C. N. Phase-coherent transport in graphene quantum billiards. *Science* **2007**, *317*, 1530–1533.
10. Zhang, Y. B.; Tan, Y. W.; Stormer, H. L.; Kim, P. Experimental observation of the quantum Hall effect and Berry's phase in graphene. *Nature* **2005**, *438*, 201–204.
11. Heersche, H. B.; Jarillo-Herrero, P.; Oostinga, J. B.; Vandersypen, L. M. K.; Morpurgo, A. F. Bipolar supercurrent in graphene. *Nature* **2007**, *446*, 56–59.
12. Morozov, S. V.; Novoselov, K. S.; Katsnelson, M. I.; Schedin, F.; Ponomarenko, L. A.; Jiang, D.; Geim, A. K. Strong suppression of weak localization in graphene. *Phys. Rev. Lett.* **2006**, *97*, 016801.
13. Pisana, S.; Lazzeri, M.; Casiraghi, C.; Novoselov, K. S.; Geim, A. K.; Ferrari, A. C.; Mauri, F. Breakdown of the adiabatic Born−Oppenheimer approximation in graphene. *Nat. Mater.* **2007**, *6*, 198–201.
14. Watcharotone, S.; Dikin, D. A.; Stankovich, S.; Piner, R.; Jung, I.; Dommett, G. H. B.; Evmenenko, G.; Wu, S. E.; Chen, S. F.; Liu, C. P.; Nguyen, S. T.; Ruoff, R. S. Graphene−silica composite thin films as transparent conductors. *Nano Lett.* **2007**, *7*, 1888–1892.
15. Gomez-Navarro, C.; Weitz, R. T.; Bittner, A. M.; Scolari, M.; Mews, A.; Burghard, M.; Kern, K. Electronic transport properties of individual chemically reduced graphene oxide sheets. *Nano Lett.* **2007**, *7*, 3499–3503.
16. Cox, P. A. *The electronic structure and chemistry of solids*; Oxford University Press: New York, 1987; p xi and 259.
17. Shi, Y. M.; Luo, S. C.; Fang, W. J.; Zhang, K. K.; Ali, E. M.; Boey, F. Y. C.; Ying, J. Y.; Wang, J. L.; Yu, H. H.; Li, L. J. Work function engineering of electrodes *via* electropolymerization of ethylenedioxythiophenes and its derivatives. *Org. Electron.* **2008**, *9*, 859–863.
18. Crispin, X.; Geskin, V.; Crispin, A.; Cornil, J.; Lazzaroni, R.; Salaneck, W. R.; Bredas, J. L. Characterization of the interface dipole at organic/metal interfaces. *J. Am. Chem. Soc.* **2002**, *124*, 8131–8141.
19. Cui, X. D.; Freitag, M.; Martel, R.; Brus, L.; Avouris, P. Controlling energy-level alignments at carbon nanotube/Au contacts. *Nano Lett.* **2003**, *3*, 783–787.
20. Zabel, P.; Dittrich, T.; Liao, Y. L.; Lin, C. Y.; Wong, K. T.; Fungo, F.; Fernandez, L.; Otero, L. Engineering of gold surface work function by electrodeposition of spirobifluorene donor−acceptor bipolar systems. *Org. Electron.* **2009**, *10*, 1307–1313.
21. Das, B.; Voggu, R.; Rout, C. S.; Rao, C. N. R. Changes in the electronic structure and properties of graphene induced by molecular charge-transfer. *Chem. Commun.* **2008**, *41*, 5155–5157.
22. Dong, X. C.; Fu, D. L.; Fang, W. J.; Shi, Y. M.; Chen, P.; Li, L. J. Doping single-layer graphene with aromatic molecules. *Small* **2009**, *5*, 1422–1426.
23. Schedin, F.; Geim, A. K.; Morozov, S. V.; Hill, E. W.; Blake, P.; Katsnelson, M. I.; Novoselov, K. S. Detection of individual gas molecules adsorbed on graphene. *Nat. Mater.* **2007**, *6*, 652–655.
24. Yu, Y. J.; Zhao, Y.; Ryu, S.; Brus, L. E.; Kim, K. S.; Kim, P. Tuning the graphene work function by electric field effect. *Nano Lett.* **2009**, *9*, 3430–3434.
25. Rao, C. N. R.; Sood, A. K.; Subrahmanyam, K. S.; Govindaraj, A. Graphene: the new two-dimensional nanomaterial. *Angew. Chem., Int. Ed.* **2009**, *48*, 7752–7777.
26. Liu, Z. F.; Liu, Q.; Huang, Y.; Ma, Y. F.; Yin, S. G.; Zhang, X. Y.; Sun, W.; Chen, Y. S. Organic photovoltaic devices based on a novel acceptor material: graphene. *Adv. Mater.* **2008**, *20*, 3924–3930.
27. Wang, X.; Zhi, L. J.; Tsao, N.; Tomovic, Z.; Li, J. L.; Mullen, K. Transparent carbon films as electrodes in organic solar cells. *Angew. Chem., Int. Ed.* **2008**, *47*, 2990–2992.
28. Su, C.-Y.; Xu, Y.; Zhang, W.; Zhao, J.; Tang, X.; Tsai, C.-H.; Li, L.-J. Electrical and spectroscopic characterizations of ultra-large reduced graphene oxide monolayers. *Chem. Mater.* **2009**, *21*, 5674–5680.

29. Kim, K. S.; Zhao, Y.; Jang, H.; Lee, S. Y.; Kim, J. M.; Kim, K. S.; Ahn, J. H.; Kim, P.; Choi, J. Y.; Hong, B. H. Large-scale pattern growth of graphene films for stretchable transparent electrodes. *Nature* **2009**, *457*, 706–710.
30. Berger, C.; Song, Z. M.; Li, X. B.; Wu, X. S.; Brown, N.; Naud, C.; Mayou, D.; Li, T. B.; Hass, J.; Marchenkov, A. N.; Conrad, E. H.; First, P. N.; de Heer, W. A. Electronic confinement and coherence in patterned epitaxial graphene. *Science* **2006**, *312*, 1191–1196.
31. Sutter, P. W.; Flege, J. I.; Sutter, E. A. Epitaxial graphene on ruthenium. *Nat. Mater.* **2008**, *7*, 406–411.
32. Reina, A.; Jia, X. T.; Ho, J.; Nezich, D.; Son, H. B.; Bulovic, V.; Dresselhaus, M. S.; Kong, J. Large area, few-layer graphene films on arbitrary substrates by chemical vapor deposition. *Nano Lett.* **2009**, *9*, 30–35.
33. Reina, A.; Thiele, S.; Jia, X.; Bhaviripudi, S.; Dresselhaus, M. S.; Schaefer, J. A.; Kong, J. Growth of large-area single- and bi-layer graphene by controlled carbon precipitation on polycrystalline Ni surfaces. *Nano Res.* **2009**, *2*, 509–516.
34. Li, X. S.; Cai, W. W.; An, J. H.; Kim, S.; Nah, J.; Yang, D. X.; Piner, R.; Velamakanni, A.; Jung, I.; Tutuc, E.; Banerjee, S. K.; Colombo, L.; Ruoff, R. S. Large-area synthesis of high-quality and uniform graphene films on copper foils. *Science* **2009**, *324*, 1312–1314.
35. Shan, B.; Cho, K. J. First principles study of work functions of single wall carbon nanotubes. *Phys. Rev. Lett.* **2005**, *94*, 236602.
36. Choi, H. C.; Shim, M.; Bangsaruntip, S.; Dai, H. Spontaneous reduction of metal ions on the sidewalls of carbon nanotubes. *J. Am. Chem. Soc.* **2002**, *124*, 9058–9059.
37. Kim, K. K.; Alfonso, R. R.; Shi, Y.; Park, H.; Li, L.-J.; Lee, Y. H.; Kong, J. Enhancing the conductivity of transparent graphene films *via* doping. *Nanotechnology*, submitted.
38. Dong, X.; Shi, Y.; Huang, W.; Chen, P.; Li, L.-J. Electrical detection of DNA hybridization with single-base specificity using transistors based on CVD-grown graphene sheets. *Adv. Mater.* **2010**, *22*, 1649–1653.
39. Wei, J. Q.; Jia, Y.; Shu, Q. K.; Gu, Z. Y.; Wang, K. L.; Zhuang, D. M.; Zhang, G.; Wang, Z. C.; Luo, J. B.; Cao, A. Y.; Wu, D. H. Double-walled carbon nanotube solar cells. *Nano Lett.* **2007**, *7*, 2317–2321.
40. Jia, Y.; Wei, J. Q.; Wang, K. L.; Cao, A. Y.; Shu, Q. K.; Gui, X. C.; Zhu, Y. Q.; Zhuang, D. M.; Zhang, G.; Ma, B. B.; Wang, L. D.; Liu, W. J.; Wang, Z. C.; Luo, J. B.; Wu, D. Nanotube−silicon heterojunction solar cells. *Adv. Mater.* **2008**, *20*, 4594–4598.
41. Filleter, T.; Emtsev, K. V.; Seyller, T.; Bennewitz, R. Local work function measurements of epitaxial graphene. *Appl. Phys. Lett.* **2008**, *93*, 133117.
42. Takahashi, T.; Tokailin, H.; Sagawa, T. Angle-resolved ultraviolet photoelectron-spectroscopy of the unoccupied band-structure of graphite. *Phys. Rev. B* **1985**, *32*, 8317–8324.
43. Datta, S. S.; Strachan, D. R.; Mele, E. J.; Johnson, A. T. C. Surface potentials and layer charge distributions in few-layer graphene films. *Nano Lett.* **2009**, *9*, 7–11.
44. Krishna, K. M.; Nukaya, Y.; Soga, T.; Jimbo, T.; Umeno, M. Solar cells based on carbon thin films. *Sol. Energy Mater. Sol. Cells* **2001**, *65*, 163–170.
45. Tongay, S.; Schumann, T.; Hebard, A. F. Graphite based Schottky diodes formed on Si, GaAs, and 4H-SiC substrates. *Appl. Phys. Lett.* **2009**, *95*, 222103.
46. Li, Z.; Kunets, V. P.; Saini, V.; Xu, Y.; Dervishi, E.; Salamo, G. J.; Biris, A. R.; Biris, A. S. Light-harvesting using high density p-type single wall carbon nanotube/n-type silicon heterojunctions. *ACS Nano* **2009**, *3*, 1407–1414.
47. Anderson, W. A.; Milano, R. A. IV characteristics for silicon Schottky solar cells. *Proc. IEEE* **1975**, *63*, 206–208.
48. Ponpon, J. P.; Siffert, P. Open-circuit voltage of MIS silicon solar cells. *J. Appl. Phys.* **1976**, *47*, 3248–3251.
49. Lee, T. C.; et al. The effect of the temperature dependence of the ideality factor on metal−semiconductor solar devices. *Semicond. Sci. Technol.* **1993**, *8*, 1357.
50. Reina, A.; Son, H. B.; Jiao, L. Y.; Fan, B.; Dresselhaus, M. S.; Liu, Z. F.; Kong, J. Transferring and identification of single- and few-layer graphene on arbitrary substrates. *J. Phys. Chem. C* **2008**, *112*, 17741–17744.